AGU PUBLICATIONS

Geophysical Research Letters

RESEARCH LETTER
10.1002/2016GL071368

Key Points:
- Ocean direct radiative forcing cannot explain the regional response to increased CO_2 in atmospheric general circulation models
- Increased CO_2 over land dominates the regional response via energy input over land and a Rossby wave teleconnection
- AGCM decompositions must be reinterpreted to include the importance of increased CO_2 over land

Supporting Information:
- Supporting Information S1

Correspondence to:
T. A. Shaw,
tas1@uchicago.edu

Citation:
Shaw, T. A., and A. Voigt (2016), Land dominates the regional response to CO_2 direct radiative forcing, *Geophys. Res. Lett.*, *43*, 11,383–11,391, doi:10.1002/2016GL071368.

Received 27 SEP 2016
Accepted 28 OCT 2016
Accepted article online 4 NOV 2016
Published online 15 NOV 2016

Land dominates the regional response to CO_2 direct radiative forcing

Tiffany A. Shaw[1] and Aiko Voigt[2,3]

[1]Department of the Geophysical Sciences, University of Chicago, Chicago, Illinois, USA, [2]Institute of Meteorology and Climate Research, Karlsruhe Institute of Technology, Karlsruhe, Germany, [3]Lamont-Doherty Earth Observatory, Columbia University, New York, NY, USA

Abstract In Atmospheric General Circulation Models (AGCMs) direct radiative forcing (increased CO_2 with fixed sea surface temperature) is an imperfect concept because land temperatures are not fixed. Here the response to direct radiative forcing is decomposed into increased CO_2 over ocean and land using an AGCM with spatially dependent CO_2. The land versus ocean response is mostly linear. Consistent with previous work, ocean direct radiative forcing decreases ocean-averaged outgoing longwave radiation, precipitation, and tropical circulation intensity; however, it cannot explain the regional response to direct radiative forcing. Increased CO_2 over land dominates the regional response via energy input over land, e.g., over deserts where there is no cloud and water vapor masking and a Rossby wave teleconnection. This mechanism operates across a range of climate perturbations, including decreased CO_2. Previous AGCM decompositions involving direct radiative forcing and indirect sea surface temperature warming must be reinterpreted to include the importance of increased CO_2 over land.

1. Introduction

The response of the climate system to increased CO_2 involves direct and indirect effects. Direct radiative forcing is defined as the response to increased CO_2 in the absence of surface temperature feedbacks [*Mitchell*, 1983; *Allen and Ingram*, 2002]. The CO_2 direct effect is typically quantified using the response to increased CO_2 in atmosphere-only models with prescribed sea surface temperature (SST) [e.g., *Mitchell*, 1983; *Mitchell et al.*, 1987; *Allen and Ingram*, 2002; *Deser and Phillips*, 2009; *Wyant et al.*, 2012; *Bony et al.*, 2013; *Merlis*, 2015] or the initial coupled climate model response to an abrupt increase in CO_2 [*Bony et al.*, 2013]. Indirect effects include changes in surface temperature that are typically quantified via uniform or patterned SST increase in atmosphere-only models [*Mitchell*, 1983; *Mitchell et al.*, 1987; *Taylor et al.*, 2012].

The decomposition into direct and indirect effects using Atmospheric General Circulation Models (AGCMs) has been used to understand the circulation response to increased CO_2 in coupled climate models. During Northern Hemisphere (NH) summer the sum of the circulation response to direct radiative forcing and indirect SST warming in AGCMs agrees with the coupled climate model response to increased CO_2 [*Shaw and Voigt*, 2015]. The summertime response includes a westward shift of the Atlantic anticyclone, which is dominated by direct radiative forcing and is important for future hurricane steering. Direct radiative forcing also weakens tropical circulation intensity and contributes to precipitation changes [*Allen and Ingram*, 2002; *Bony et al.*, 2013; *Medeiros et al.*, 2015]. During NH winter the extratropical circulation response to increased CO_2 is dominated by indirect SST warming [*He et al.*, 2014; *Grise and Polvani*, 2014].

The decomposition into direct radiative forcing and indirect SST warming using AGCMs is imperfect because land temperatures are not fixed; i.e., the concept of direct radiative forcing only applies over the ocean. In response to direct radiative forcing there is a small increase in land temperature that can impact clouds and the circulation [*Wyant et al.*, 2012; *Bony et al.*, 2013]. While the impact of increased CO_2 over land has been assessed qualitatively by comparing AGCM and aquaplanet responses over the ocean [*Bony et al.*, 2013; *Medeiros et al.*, 2015], the impact of land has not been assessed quantitatively.

A systematic comparison of the response to increased CO_2 over ocean versus land in AGCMs is necessary for understanding the mechanisms of the circulation response to direct radiative forcing. Previous work has shown that direct radiative forcing can impact the ocean-averaged circulation by weakening net radiative

cooling and stabilizing the atmosphere [*Bony et al.*, 2013] and by cloud and water vapor masking [*Merlis*, 2015]. However, energetic responses to radiative perturbations over ocean and land are different in AGCMs. Over land, surface temperatures are interactive and the surface energy budget is closed. Hence, top of the atmosphere (TOA) radiative perturbations directly perturb energy input to the atmosphere (EIA) and moist static energy transport. In contrast, over ocean, where surface temperatures are fixed, TOA perturbations can be compensated by a change in the surface energy budget leading to small changes in EIA and moist static energy transport. Note that there can still be changes in the circulation, but they must be compensated by changes in stratification.

Here we use novel AGCM simulations with spatially dependent CO_2 to decompose the direct radiative forcing response into contributions from increased CO_2 over ocean (ocean direct radiative forcing) and land. We address the following questions: Does ocean direct radiative forcing explain the thermodynamic and circulation response to direct radiative forcing in AGCMs? What mechanism dominates the circulation response to direct radiative forcing? The AGCM simulations are described in section 2. Our results are presented in section 3 and summarized in section 4.

2. Methods

We make use of AGCM simulations from the Coupled Model Intercomparison Project Phase 5 (CMIP5) archive [*Taylor et al.*, 2012], in particular, the AMIP, AMIP4xCO_2 (hereafter AMIP4x), and AMIP4K experiments. AMIP is the standard AGCM protocol with prescribed historical forcings (i.e., radiative forcing, SST, sea ice, etc.) from 1979 to 2008 [*Gates et al.*, 1999]. AMIP4x involves quadrupling the AMIP CO_2 while holding SSTs fixed. Following previous work, we refer to this experiment as "direct radiative forcing" (CO_2 direct effect) or the response to increased CO_2 where fixed SSTs are assumed. In contrast, AMIP4K involves increasing SSTs by 4K while holding CO_2 fixed. We use monthly data from 10 CMIP5 AGCMs (bcc-csm1-1, CanAM4, CNRM-CM5, HadGEM2-A, IPSL-CM5A-LR, IPSL-CM5B-LR, MIROC5, MPI-ESM-LR, MPI-ESM-MR, and MRI-CGCM3) that performed the AMIP, AMIP4x, and AMIP4K experiments.

We also conduct simulations with the MPI-ESM-LR, hereafter referred to as MPI, AGCM [*Stevens et al.*, 2013]. The MPI AGCM AMIP4x-AMIP response is consistent with the CMIP5 ensemble (compare Figure 1 (left) to Figure S1 in the supporting information), in particular, there is a westward shift of the Atlantic anticyclone and a poleward shift of the Pacific jet (Table 1). The MPI AGCM is configured to include spatially dependent (latitude and longitude) CO_2; i.e., the CO_2 concentration is prescribed separately in each grid column. The spatially dependent CO_2 is used to separately quantify the response to increased CO_2 only over ocean (ocean direct radiative forcing) from increased CO_2 only over land with fixed SSTs. We note that separating the CO_2 increase geographically may lead to nondirect effects, e.g., generating gradients of radiative forcing; however, this concern is minimized by the fact that the response to increased CO_2 over land and ocean is mostly linear. The response to increased CO_2 over land involves radiation and vegetation contributions. The radiation and vegetation contributions are isolated via increased CO_2 in the radiation or land surface schemes, respectively. Finally, we quantify the response to increased CO_2 over eastern versus western hemisphere continents. Table 1 lists the various MPI experiments.

We focus on the response to increased CO_2 in the MPI AGCM during NH summer (June, July, and August), which includes changes in the Monsoons. *Shaw and Voigt* [2015] showed the sum of AGCM direct radiative forcing, and indirect SST warming responses agree with coupled climate models during summer. All of the results discussed below also apply to SH summer (December, January, and February) and annual mean responses. Finally, the response to increased CO_2 is discussed in terms of the effective radiative forcing, i.e., including rapid tropospheric and surface adjustments [*Sherwood et al.*, 2015]. The effective radiative forcing is more relevant than instantaneous forcing when interpreting circulation changes in AGCMs where SSTs are prescribed but land temperatures are interactive.

3. Results

3.1. Response to Ocean Direct Radiative Forcing

Direct radiative forcing weakens radiative cooling of the atmosphere, which is expected to decrease precipitation [*Allen and Ingram*, 2002] and slow down tropical circulation intensity over the ocean [*Bony et al.*, 2013]. The spatial pattern of TOA radiative changes due to direct radiative forcing can also be influenced by clouds

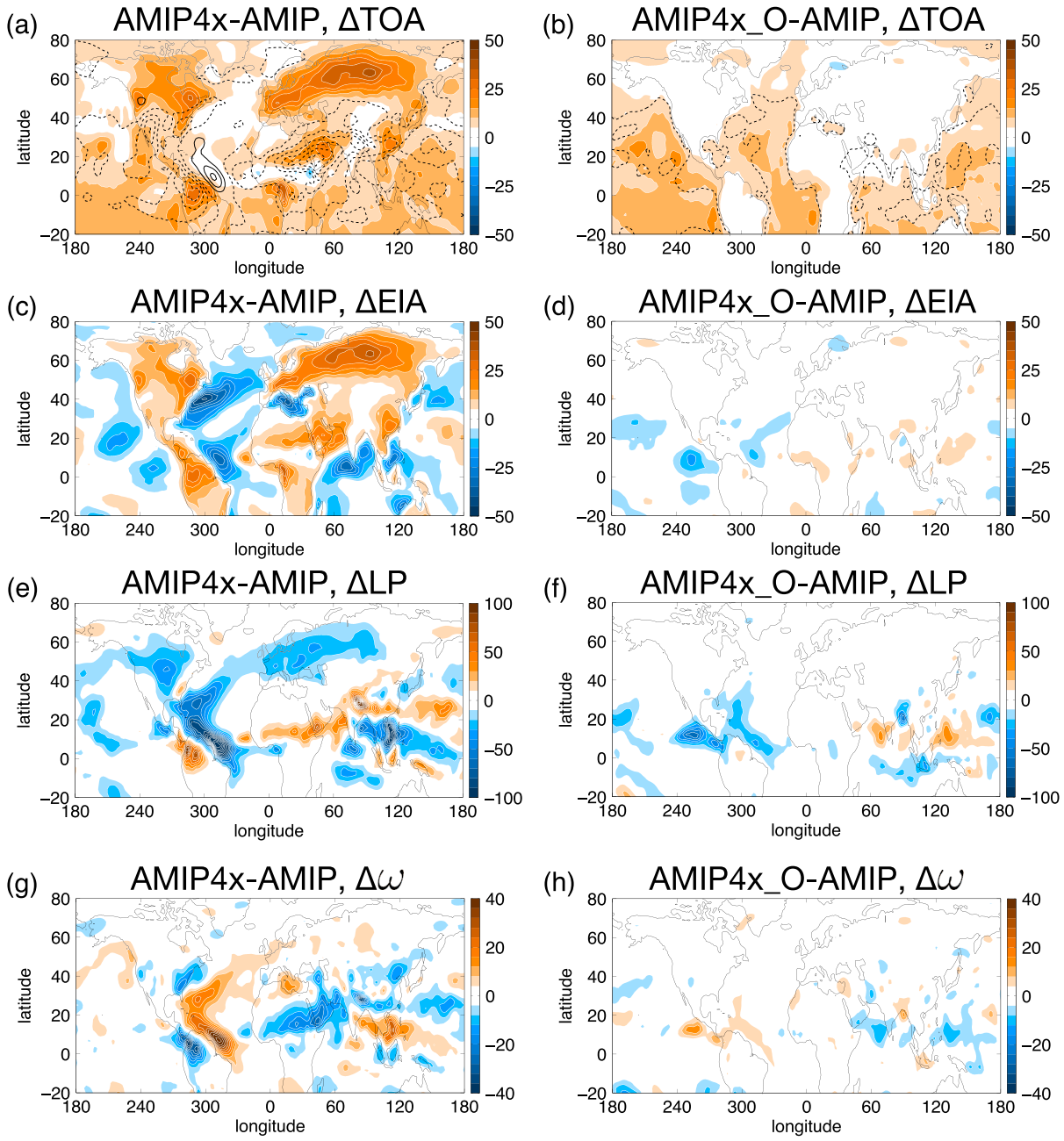

Figure 1. Response of summertime (June, July, and August) (a, b) TOA radiation (shading) and OLR (contours), (c, d) EIA, (e, f) precipitation (weighted by latent heat of vaporization), and (g, h) 500 hPa ω to increased CO_2 everywhere (left) and ocean direct radiative forcing (right) in the MPI AGCM. Contour interval is 2.5 W m^{-2} (Figures 1a–1f), (g, h) 4.0 hPa day^{-1}.

and water vapor masking [*Merlis*, 2015]. We begin by evaluating the response to ocean direct radiative forcing in the MPI AGCM and assess whether the above mechanisms explain the response when CO_2 increases everywhere (AMIP4x-AMIP).

Ocean direct radiative forcing increases TOA radiation (TOA = $S_{TOA} - L_{TOA}$ where S_{TOA} is net incoming shortwave radiation and L_{TOA} is OLR) over the ocean (Figure 1b, shading) primarily due to decreased OLR (Figure 1b, contours). TOA radiation increases by 13.43% in regions of climatological ascent over the ocean and by 27.86% in regions of descent, suggesting that cloud and water vapor masking is important. The TOA increase is compensated by decreased surface heat fluxes; consequently, ocean direct radiative forcing has a small impact on

Table 1. MPI AGCM Simulation Description and Shifts of the Circulation[a]

Simulation	Description	$\Delta\phi_{EFE}$ (°N)	$\Delta\phi_{TE}$ (°N)	$\Delta\phi_{AA}$ (°E)	$\Delta\phi_{Pac}$ (°N)
AMIP4x	4xCO_2 everywhere	1.3°	2.8°	−5.8°	1.4°
AMIP4x_O	4xCO_2 ocean	0.2°	−0.1°	−1.1°	−0.2°
AMIP4x_L	4xCO_2 land	1.0°	2.5°	−4.9°	1.8°
AMIP4x_LR	4xCO_2 land radiation	0.8°	1.4°	−3.5°	1.2°
AMIP4x_LV	4xCO_2 land vegetation	0.1°	0.8°	−1.3°	0.5°
AMIP4x_LRE	4xCO_2 Eastern hemisphere land	0.6°	0.8°	−3.3°	0.8°
AMIP4x_LRW	4xCO_2 Western hemisphere land	0.0°	0.5°	−0.7°	0.3°

[a]Shift of the moist static energy flux equator ($\Delta\phi_{EFE}$), latitude of maximum transient-eddy moist static energy flux in the NH ($\Delta\phi_{TE}$), longitude of Atlantic anticyclone from 20 to 50°N ($\Delta\phi_{AA}$), and latitude of North Pacific jet ($\Delta\phi_{Pac}$), in response to increased CO_2. For comparison, the CMIP5 AMIP4xCO_2-AMIP multimodel mean shifts are $\Delta\phi_{EFE}$=1.0°N, $\Delta\phi_{AA}$=−4.8°E and $\Delta\phi_{Pac}$=1.2°N

EIA (EIA=TOA − SFC where SFC=S_{SFC} − L_{SFC} − LH − SH where S_{SFC} is net surface shortwave radiation, L_{SFC} is net surface longwave radiation, LH is latent heat flux and SH is sensible heat flux (Figure 1d), as expected.

Ocean direct radiative forcing decreases ocean-averaged precipitation (Figure 1f, $\Delta\{P\}/\{P\}$=−3.57% where $\{\cdot\}$ represents an average over the ocean); however, this only accounts for about half of the ocean-averaged precipitation decrease when CO_2 increases everywhere (Figure 1e, $\Delta\{P\}/\{P\}$=−6.91%). Consistent with the precipitation decrease, ocean direct radiative forcing weakens tropical circulation intensity over the ocean defined as $I = \hat{\omega}^{\downarrow} - \hat{\omega}^{\uparrow}$, where $\hat{\omega}^{\downarrow}$ is the tropical average (35°S–35°N) of downward $\hat{\omega}$ (the vertically averaged vertical velocity between 1000 and 100 hPa), and $\hat{\omega}^{\uparrow}$ is the average of upward values (Figure 1h, $\Delta I/I$=−1.43%). This also represents about half of the ocean-averaged weakening when CO_2 increases everywhere (Figure 1g, $\Delta I/I$=−2.50%).

Overall, the ocean-averaged response to ocean direct radiative forcing agrees with the mechanisms discussed above. However, ocean direct radiative forcing cannot explain the regional radiation, precipitation,and vertical velocity response when CO_2 increases everywhere in the MPI AGCM (compare Figures 1, left and 1, right). Furthermore, it does not dominate the westward shift of the Atlantic anticyclone and the poleward shift of the Pacific jet stream (Table 1). Since the response to increased CO_2 is linear when decomposed into ocean and land contributions (Figure S2), we turn to the response to increased CO_2 over land to understand the response when CO_2 increases everywhere.

3.2. Response to Increased CO_2 Over Land

How is the response to increased CO_2 over land different from ocean direct radiative forcing? What mechanisms account for the circulation response to increased CO_2 over land? Increased CO_2 over land increases TOA radiation over land (Figure 2a, shading) due to (i) decreased OLR in low latitudes (Figure 2a, contours) and (ii) increased net shortwave (decreased albedo) in middle and high latitudes. The TOA radiation changes are small in regions of deep convection (African and Indian Monsoon regions) consistent with cloud and water vapor masking [*Merlis*, 2015]. However, the cloud masking results from changes in TOA cloud radiative effect (CRE, Figure S3, see also *Wyant et al.* [2012]) rather than from the presence of climatological clouds. Over desert regions in the Middle East and North Africa, TOA radiation increases because there is no cloud or water vapor masking.

The TOA radiation increase over land is not compensated by surface radiation and heat flux changes; consequently, EIA increases over land (Figure 2b). In addition, EIA decreases over the ocean in response to increased CO_2 over land (Figure 2b) due to decreased surface latent heat flux. This is an example of a land-ocean teleconnection that we will discuss further below. A similar land-ocean teleconnection exists in response to indirect SST warming, namely, EIA increases over ocean but decreases over land (Figure S4). The radiative contribution of increased CO_2 over land dominates over the vegetation contribution in most regions, the exceptions being the Gulf Stream and Northern Eurasia (Figure S5). The vegetation contribution also decreases precipitation over North America and Europe.

Increased CO_2 over land decreases ocean-averaged precipitation (Figure 2c, $\Delta\{P\}/\{P\}$=−3.31%) primarily due to increased descent over the tropical oceans via the land-ocean teleconnection. Consistent with the

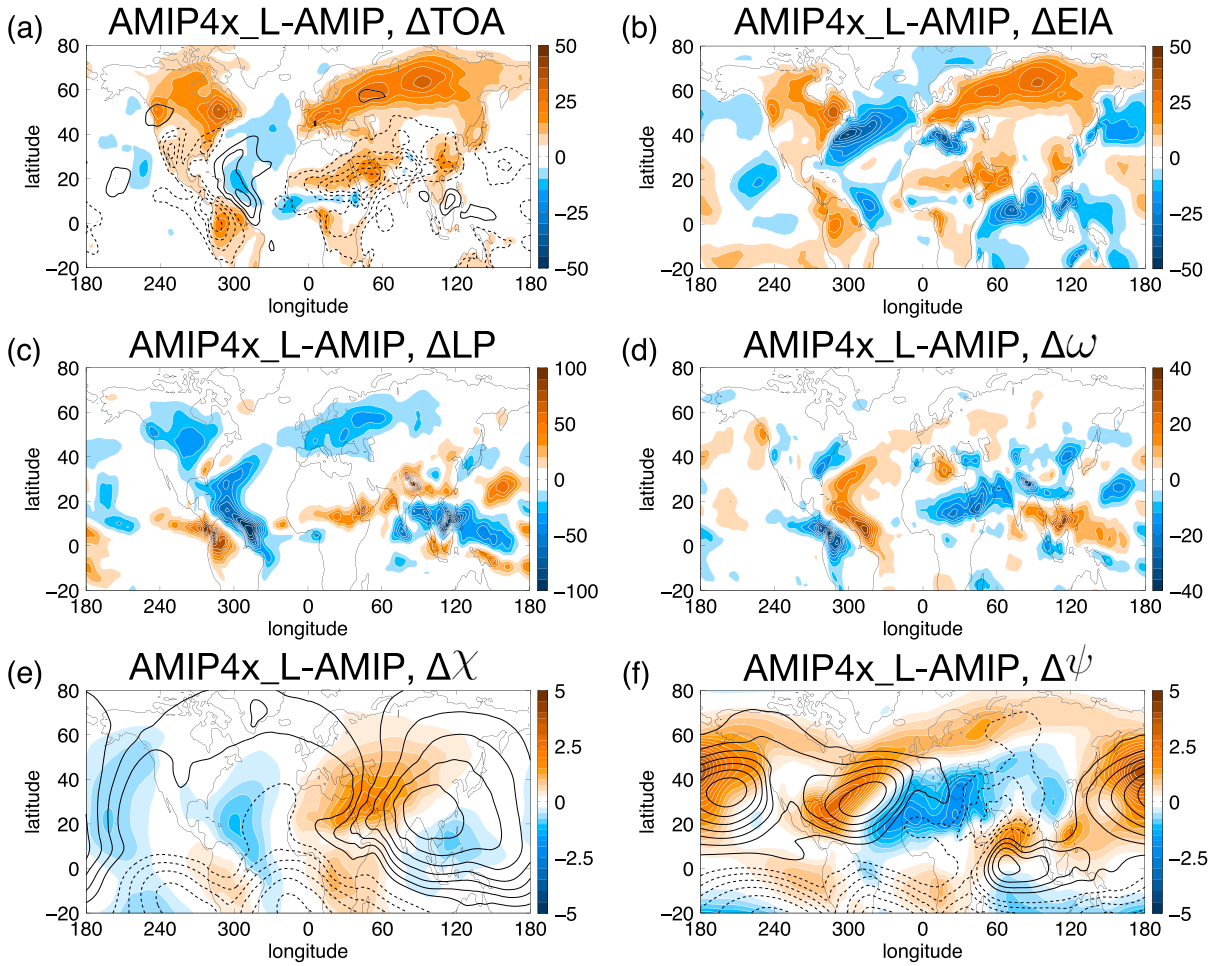

Figure 2. Response of summertime (a) TOA radiation (shading) and OLR (contours), (b) EIA, (c) precipitation (weighted by latent heat of vaporization), (d) 500 hPa ω, (e) 925 hPa velocity potential, and (f) 925 hPa stream function (shading) to increased CO_2 over land in the MPI AGCM. In Figures 2e and 2f contours (negative dashed) indicate the AMIP climatology. Contour interval for Figures 2a–2d is similar to Figure 1; 2.5e5 $m^2\ s^{-1}$ (shading) and 2.0e6 $m^2\ s^{-1}$ (black) (Figures 2e and 2f).

linearity of the response to increased CO_2 over land and ocean, this represents about half of the ocean-averaged precipitation decreased when CO_2 increases everywhere (Figure 1e, $\Delta\{P\}/\{P\} = -6.91\%$). There are also significant regional changes, including increased precipitation and precipitation minus evaporation over Monsoon regions (Figure 2c). Following energy and moisture balance constraints, the EIA and precipitation minus evaporation responses to increased CO_2 over land imply energy and moisture flux convergence over land and divergence over ocean, which shifts the energy flux equator (EFE, where moist static energy transport is zero in the tropics [see *Schneider et al.*, 2014]) northward. The northward EFE shift is due to increased energy transport across 10°N (we follow equation (1) in *Shaw et al.* [2015], which is based on the framework of *Bischoff and Schneider* [2014], but use a reference latitude of 10°N rather than the equator because the climatological EFE is at 14.45°N during NH summer). The latitude of maximum zonal-mean transient eddy energy transport, which is determined by the storm tracks, also shifts northward. (There is no significant shift of the latitude of maximum transient eddy transport in the SH.) These shifts are dominated by increased CO_2 over land (Table 1).

Previous work has shown that circulation changes dominate the moisture transport response to direct radiative forcing (i.e., the dynamic contribution defined following *Clement et al.* [2004] and *Seager et al.* [2010] dominates) in the CMIP5 ensemble [see *Shaw and Voigt*, 2015, Figure S1]. Circulation changes also dominate the moisture transport response to increased CO_2 over land in the MPI AGCM. Ocean direct radiative forcing mechanisms cannot explain the circulation response to increased CO_2. Another potential mechanism is the Monsoon-desert mechanism [*Rodwell and Hoskins*, 1996, 2001; *Wang and Ting*, 1999]. This mechanism couples the divergent and rotational flow. During summertime near-surface climatological convergence in regions of

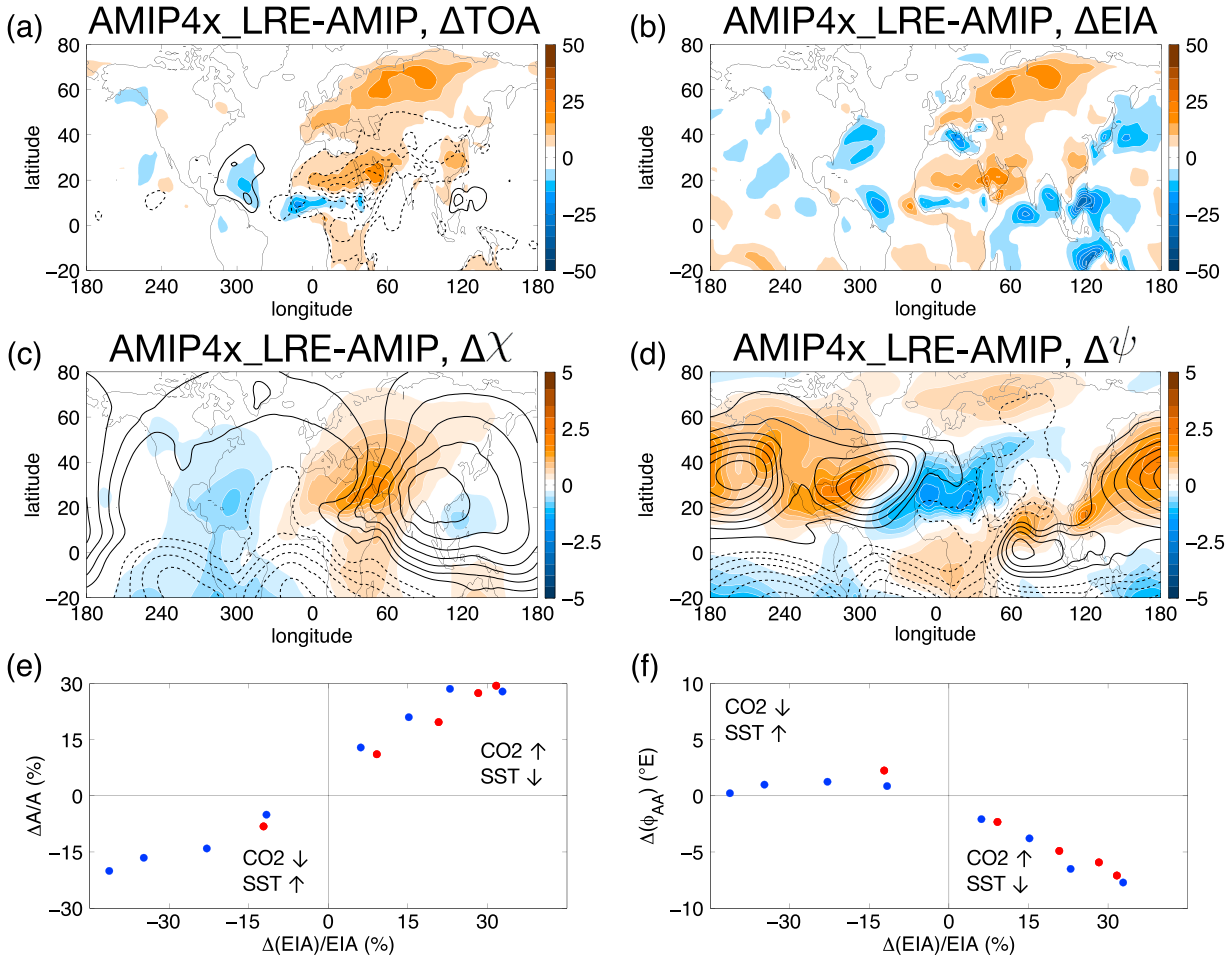

Figure 3. Response of summertime (a) TOA radiation (shading) and OLR (contours) (b) EIA, (c) 925 hPa velocity potential, and (d) 925 hPa stream function to increased CO_2 over eastern hemisphere land in the MPI AGCM. Contouring as in Figure 2. Response of summertime (e) amplitude of rotational flow and (f) position of Atlantic anticyclone versus EIA over eastern hemisphere land across a range of climate perturbations in the MPI AGCM. Red circles indicate CO_2 changes whereas blue circles indicate SST changes.

positive velocity potential is coupled to ascent and cyclonic circulations over the African and Asian Monsoon (black contours in Figures 2e and 2f). The corresponding divergence in regions of negative velocity potential is coupled to descent and anticyclonic circulation to the west (over the Mediterranean, Atlantic, and East Pacific) via a Rossby wave response [*Rodwell and Hoskins*, 2001; *Sardeshmukh and Hoskins*, 1998]. The regions of descent over the eastern ocean basins are associated with strong temperature inversions capping the boundary layer and SST coupling [*Seager et al.*, 2003].

The divergent and rotational flow response to increased CO_2 over land is consistent with the Monsoon-desert mechanism. In particular, convergence and ascent increase over the Middle East and North Africa (consistent with increased EIA over deserts) and South East Asia (Figures 2d–2f). Divergence and descent occur to the west over the Atlantic, Pacific, and Indian oceans consistent with decreased EIA (Figures 2d and 2e). In addition, there is an anomalous cyclonic circulation over the Middle East and North Africa and an anomalous anticyclonic circulation over the western Atlantic and Pacific (Figure 2f). The summertime rotational flow, defined as the squared stream function ($A = \psi^2$) amplifies in response to increased CO_2 over land ($\Delta A/A = 19.2\%$). The westward shift of the Atlantic anticyclone and poleward shift of the Pacific jet stream are consistent with this amplification and also with a westward shift of the velocity potential (Figure 2e). Since the ascent and increased velocity potential in response to increased CO_2 over land occurs over primarily deserts (not over Monsoon regions), it is confusing to refer to the Monsoon-desert mechanism in the context of the response to increased CO_2, instead we will refer to it as the Rossby wave teleconnection.

The causality of the Rossby wave teleconnection can be isolated using the response to increased CO_2 over eastern hemisphere land. Increased CO_2 over eastern hemisphere land increases TOA radiation and EIA over deserts (Middle East and North Africa) and Southeast Asia (Figures 3a and 3b). Increased EIA is associated with increased velocity potential, ascent, and cyclonic circulation (Figures 3c and 3d). The corresponding negative velocity potential, descent, and anticyclonic circulation occur to the west over the Atlantic and Pacific Oceans (Figures 3c and 3d) where EIA decreases. The response to increased CO_2 over eastern hemisphere land dominates the westward shift of the Atlantic anticyclone and poleward shift of the Pacific jet stream (Table 1). Increased CO_2 over western hemisphere land is important for increasing EIA over South America and inducing a Rossby wave response over the Pacific Ocean (Figure S6). However, the circulation response over North America is dominated by increased CO_2 over eastern hemisphere land consistent with the eastern hemisphere having a larger land area.

3.3. Response Across a Range of Climate Perturbations

The results in the previous sections show that increased CO_2 over land dominates the regional response to direct radiative forcing in the MPI AGCM via its impact on EIA over land. *Shaw and Voigt* [2016] showed that changes in EIA over land can be connected to changes in the divergent and rotational flow using the moist static energy budget and a simple boundary layer model. They illustrated the connection in aquaplanet simulations whereby increased EIA over idealized aquaplanet land amplified the rotational flow and decreased EIA over land weakened it [see *Shaw and Voigt*, 2016, Figures 6d and 7d]. Here we examine the connection between EIA over eastern hemisphere land and rotational flow, including the position of the Atlantic anticyclone in the MPI AGCM. We run additional simulations with different climate perturbations; e.g., CO_2 is increased over land by 0.5, 2, 4, 6, and 8 times AMIP CO_2 with fixed SST, and SST is changed from ± 2 to ± 8 K with fixed CO_2. (The MPI AGCM would not run with CO_2 concentrations less than 0.5 times the AMIP CO_2.)

Across the range of climate perturbations, the rotational flow amplitude ($\Delta A/A$) changes almost linearly with EIA over eastern hemisphere land. In particular, increased EIA over eastern hemisphere land in response to increased CO_2 (Figure 3e, red circles, top right quadrant) or decreased SST (Figure 3e, blue circles, top right quadrant) amplify the rotational flow in the NH. In contrast, decreased EIA over eastern hemisphere land in response to decreased CO_2 (Figure 3e, red circle, bottom left quadrant) or increased SST (Figure 3e, blue circles, bottom left quadrant) weaken the rotational flow in the NH. In addition, increased EIA over land due to increased CO_2 over land (Figure 3f, red circle, bottom right) or decreased SST (Figure 3f, blue circles, bottom right) shifts the Atlantic anticyclone westward. Decreased EIA over land due to decreased CO_2 shifts the Atlantic anticyclone eastward (Figure 3f, red circle, top left) but SST warming does not significantly impact the Atlantic anticyclone [*Shaw and Voigt*, 2015]. The response to SST warming involves thermodynamic energy transport changes, including changes in gross moist stability, which can oppose the dynamic response in some regions.

4. Conclusion and Discussion

Direct radiative forcing, defined as the response to increased CO_2 in the absence of surface temperature changes, plays an important role in the transient and equilibrium coupled climate model response to increased CO_2. However, in AGCMs the direct radiative forcing concept is imperfect because land temperatures are not fixed. Here AGCM simulations with spatially dependent CO_2 were used to separately quantify the impact of increased CO_2 over ocean and land with fixed SSTs. Our conclusions can be summarized as follows.

1. Ocean direct radiative forcing decreases ocean-averaged OLR, precipitation, and vertical motion consistent with weaker net radiative cooling. However, it does not explain the regional radiation, precipitation, and circulation response when CO_2 is increased everywhere.
2. The response to increased CO_2 over ocean and land is mostly linear; i.e., sum agrees with the response to direct radiative forcing (increased CO_2 everywhere). Consequently, increased CO_2 over land dominates the regional radiation, precipitation, and circulation response.
3. Ocean direct radiative forcing has a small impact on EIA because surface fluxes compensate TOA changes. In contrast, surface fluxes do not compensate TOA changes over land; thus, increased CO_2 over land increases EIA over land. The EIA increase over land results from (i) an increase in desert regions where there is no cloud and water vapor masking and (ii) decreased albedo over middle and high latitudes. In addition, EIA decreases over the ocean, due to decreased latent heat fluxes via the land-ocean teleconnection.

4. The circulation response to increased CO_2 over land is consistent with a Rossby wave teleconnection driven by EIA changes over land. Increased EIA drives ascent and increased velocity potential in response to increased CO_2 over eastern hemisphere land, which is coupled to descent and decreased velocity potential over the ocean via a Rossby wave response. This mechanism produces robust circulation changes, including a poleward shift of the EFE, NH storm track and Pacific jet, amplification of the rotational flow, and a westward shift of the Atlantic anticyclone. The westward shift of ascent and increased velocity potential toward the deserts explains the westward shift of the Atlantic anticyclone, which is important for future hurricane steering.
5. The connection between EIA over land, rotational flow amplitude, and Atlantic anticyclone position operates over a range of climate perturbations in the MPI AGCM, including decreased CO_2 and SST.

An important consequence of these results is that previous decompositions of the circulation response into direct radiative forcing and indirect SST warming (fast and slow) contributions [e.g., *Bony et al.*, 2013; *Grise and Polvani*, 2014; *Merlis*, 2015; *Shaw and Voigt*, 2015] must be reinterpreted to account for the importance of increased CO_2 over land. The results confirm the hypothesis of *Shaw and Voigt* [2015] that increased CO_2 over land dominates the circulation response to direct radiative forcing. While we consider our conclusions robust given the agreement of the MPI AGCM response with the CMIP5 AGCM ensemble, an assessment in other models is needed. The linearity of the response to increased CO_2 over land and ocean is surprising; however, it is consistent with previous single-forcing experiments that documented the additivity of the circulation response to ozone and CO_2 changes [*McLandress et al.*, 2011; *Polvani et al.*, 2011].

The results highlight an important Rossby wave land-ocean teleconnection in response to increased CO_2 over land. In particular, decreased EIA over the ocean, which is consistent with reduced convergence, precipitation, and weakening of the circulation, occurs in response to increased CO_2 over land. The teleconnection dominates in the summer hemisphere when climatological energy input over land is positive. The land-ocean teleconnection in response to increased CO_2 is complementary to the teleconnection in response to indirect SST warming. For example, indirect SST warming decreases EIA and amplifies the temperature response over land [*Sutton et al.*, 2007] due to different lapse rates over land and ocean and a teleconnection involving the weak temperature gradient approximation [*Joshi et al.*, 2013; *Byrne and O'Gorman*, 2013].

Our AGCM simulations with spatially dependent CO_2 reveal that the land-ocean teleconnection, which couples land EIA changes to rotational flow (Rossby wave) amplitude and position of the Atlantic anticyclone, operates across a range of climate perturbations, including decreased CO_2 and decreased SST. This connection between EIA and Rossby waves is consistent with aquaplanet model results [*Shaw and Voigt*, 2016] and suggests that the teleconnection might operate in past climates when CO_2 and SSTs were different. Furthermore, the EIA response to increased CO_2 over land highlights the potential for using the seasonal cycle, where land EIA increases from winter to summer, as an emergent constraint, which is a work in progress. All of these connections emphasize the important role land plays in response to climate perturbations across a range of time scales.

Acknowledgments

T.A.S. and A.V. thank Brian Medeiros for help with the tropical circulation intensity calculation. T.A.S. is supported by the David and Lucile Packard Foundation, NSF award AGS-1538944 and the Alfred P. Sloan Foundation. A.V. is supported by the German Federal Ministry of Education and Research (BMBF) and FONA: Research for Sustainable Development (www.fona.de) under grant agreement 01LK1509A. The MPI AGCM simulations were completed with resources provided by the University of Chicago Research Computing Center and the data are available from T.A.S. upon request (tas1@uchicago.edu). We thank two anonymous reviewers whose comments helped to improve the submitted manuscript. We also thank N. Henderson and H. Liu for help downloading the CMIP5 data. We acknowledge the World Climate Research Programme's Working Group on Coupled Modelling, which is responsible for CMIP, and we thank the climate modeling groups for producing and making available their model output. For CMIP the U.S. Department of Energy's Program for Climate Model Diagnosis and Intercomparison provides coordinating support and led development of software infrastructure in partnership with the Global Organization for Earth System Science Portals (http://cmip-pcmdi.llnl.gov/cmip5/data_portal.html).

References

Allen, M. R., and W. J. Ingram (2002), Constraints on future changes in climate and the hydrological cycle, *Nature*, *419*, 224–232.

Bischoff, T., and T. Schneider (2014), Energetic constraints on the position of the intertropical convergence zone, *J. Clim.*, *27*, 4937–4951.

Bony, S., G. Bellon, D. Klocke, S. Sherwood, S. Fermepin, and S. Denvil (2013), Robust direct effect of carbon dioxide on tropical circulation and regional precipitation, *Nat. Geosci.*, *6*, 447–451, doi:10.1038/NGEO1799.

Byrne, M., and P. A. O'Gorman (2013), Land-ocean warming contrast over a wide range of climates: Convective quasi-equilibrium theory and idealized simulations, *J. Clim.*, *26*, 4000–4016.

Clement, A., A. Hall, and T. Broccoli (2004), The importance of precessional signals in the tropical climate, *Clim. Dyn.*, *22*, 327–341.

Deser, C., and A. S. Phillips (2009), Atmospheric circulation trends, 1950–2000: The relative roles of sea surface temperature forcing and direct atmospheric radiative forcing, *J. Clim.*, *22*, 396–413.

Gates, W. L., et al. (1999), An overview of the results of the Atmospheric Model Intercomparison Project (AMIP I), *Bull. Am. Meteorol. Soc.*, *80*, 29–55.

Grise, K., and L. M. Polvani (2014), The response of midlatitude jets to increased CO_2: Distinguishing the roles of sea surface temperature and direct radiative forcing, *Geophys. Res. Lett.*, *41*, 6863–6871, doi:10.1002/2014GL061638.

He, J., B. J. Soden, and B. Kirtman (2014), The robustness of the atmospheric circulation and precipitation response to future anthropogenic surface warming, *Geophys. Res. Lett.*, *41*, 2614–2622, doi:10.1002/2014GL059435.

Joshi, M. M., F. H. Lambert, and M. J. Webb (2013), An explanation for the difference between twentieth and twenty-first century land-sea warming ratio in climate models, *Clim. Dyn.*, *41*, 1853–1869.

McLandress, C., T. G. Shepherd, J. F. Scinocca, D. A. Plummer, M. Sigmond, A. I. Jonsson, and MC. Reader (2011), Separating the dynamical effects of climate change and ozone depletion. Part II: Southern Hemisphere troposphere, *J. Clim.*, *24*, 1850–1868.

Medeiros, B., B. Stevens, and S. Bony (2015), Using aquaplanets to understand the robust responses of comprehensive climate models to forcing, *Clim. Dyn.*, *44*, 1957–1977.

Merlis, T. M. (2015), Direct weakening of tropical circulations from masked CO_2 radiative forcing, *Proc. Natl. Acad. Sci. U.S.A.*, *112*, 13167–13171.
Mitchell, J. F. B. (1983), The seasonal response of a general circulation model to changes in CO_2 and sea temperatures, *Q. J. R. Meteorol. Soc.*, *109*, 113–152.
Mitchell, J. F. B., C. A. Wilson, and W. M. Cunnington (1987), On CO_2 climate sensitivity and model dependence of results, *Q. J. R. Meteorol. Soc.*, *113*, 293–322.
Polvani, L. M., D. W. Waugh, G. J. P. Correa, and S.-W. Son (2011), Stratospheric ozone depletion: The main driver of twentieth-century atmospheric circulation changes in the Southern Hemisphere?, *J. Clim.*, *24*, 210–227.
Rodwell, M. J., and B. J. Hoskins (1996), Monsoons and the dynamics of deserts, *Q. J. R. Meteorol. Soc.*, *122*, 1385–1404.
Rodwell, M. J., and B. J. Hoskins (2001), Subtropical anticyclones and summer monsoons, *J. Clim.*, *15*, 3192–3211.
Sardeshmukh, P., and B. J. Hoskins (1998), Generation of global rotational flow by steady idealized tropical divergence, *J. Atmos. Sci.*, *45*, 1228–1250.
Schneider, T., T. Bishoff, and G. H. Haug (2014), Migration and dynamics of the Intertropical Convergence Zone, *Nature*, *513*, 45–53, doi:10.1038/nature13636.
Seager, R., R. Murtugudde, N. Naik, A. Clement, N. Gordon, and J. Miller (2003), Air-sea interaction and the seasonal cycle of the subtropical anticyclones, *J. Clim.*, *16*, 1948–1966.
Seager, R., N. Naik, and G. A. Vecchi (2010), Thermodynamic and dynamic mechanisms for large-scale changes in the hydrological cycle in response to global warming, *J. Clim.*, *23*, 4651–4668.
Shaw, T. A., and A. Voigt (2015), Tug of war on summertime circulation between radiative forcing and sea-surface warming, *Nat. Geosci.*, *6*, 447–451, doi:10.1038/NGEO1799.
Shaw, T. A., and A. Voigt (2016), Understanding the links between subtropical and extratropical circulation responses to climate change using aquaplanet model simulations, *J. Clim.*, *29*, 6637–6657.
Shaw, T. A., A. Voigt, S. Kang, and J. Seo (2015), Response of the intertropical convergence zone to zonally asymmetric subtropical surface forcings, *Geophys. Res. Lett.*, *42*, 9961–9969, doi:10.1002/2015GL066027.
Sherwood, S., S. Bony, O. Boucher, C. Bretherton, P. Forster, J. Gregory, and B. Stevens (2015), Adjustments in the forcing-feedback framework for understanding climate change, *Bull. Am. Meteorol. Soc.*, *96*, 217–228.
Stevens, B., et al. (2013), Atmospheric component of the MPI-M Earth System Model: ECHAM6, *J. Adv. Model. Earth Syst.*, *5*, 146–172.
Sutton, R. T., B. Dong, and J. M. Gregory (2007), Land/sea warming ratio in response to climate change: IPCC AR4 model results and comparison with observations, *Geophys. Res. Lett.*, *34*, L02701, doi:10.1029/2006GL028164.
Taylor, K. E., R. J. Stouffer, and G. A. Meehl (2012), An overview of CMIP5 and the experiment design, *Bull. Am. Meteorol. Soc.*, *93*, 485–498, doi:10.1175/BAMS-D-11-00094.1.
Wang, H., and M. Ting (1999), Seasonal cycle of the climatological stationary waves in the NCEP-NCAR reanalysis, *J. Atmos. Sci.*, *56*, 3892–3919.
Wyant, M., C. S. Bretherton, P. N. Blossey, and M. Khairoutdinov (2012), Fast cloud adjustment to increasing CO_2 in a superparameterized climate model, *J. Adv. Model. Earth Syst.*, *4*, M05001, doi:10.1029/2011MS000092.